Electronic Supplementary Material (ESI) for Catalysis Science & Technology.
This journal is © The Royal Society of Chemistry 2018

Supporting Information

Ligand-Functionalized Pt Nanoparticles as Asymmetric Heterogeneous Catalysts: Molecular Reaction Control by Ligand-Reactant Interactions

Anda Šulce[1], Jana Backenköhler[2], Imke Schrader[1], Massimo Delle Piane[3], Christian Müller[3], André Wark[3], Lucio Colombi Ciacchi[3], Vladimir Azov,[4] Sebastian Kunz*[1]

[1]Institute of Applied and Physical Chemistry (IAPC), Center for Environmental Research and Sustainable Technology, University of Bremen, Leobener Straße, 28359 Bremen, Germany

[2]Institute for Organic and Analytical Chemistry, University of Bremen, Leobener Straße 7, 28359 Bremen, Germany

[3]Hybrid Materials Interfaces Group, Faculty of Production Engineering, Bremen Center for Computational Materials Science (BCCMS), University of Bremen, Am Fallturm 1, 28359 Bremen, Germany

[4]Department of Chemistry, University of the Free State, PO Box 339, Bloemfontein 9300, South Africa

* Corresponding Author:
Dr. Sebastian Kunz
University of Bremen
Institute of Applied and Physical Chemistry (IAPC)
D-28359 Bremen
Tel: +49-421-218 63187
eMail: SebKunz@uni-bremen.de

1. ^{1}H NMR Spectroscopic Investigation of Ligand-functionalized Pt Nanoparticles (NPs)

Ligand-functionalized Pt NPs dispersed in D_2O were investigated by ^{1}H NMR spectroscopy to probe if the ligands are tightly bound to the particle surface. Prior to performing the measurements the samples were precipitated with acetone and rinsed with EtOH in order to remove residual non-binding ligands (see experimental section 2.2). The method has been previously demonstrated to be effective for several ligands[1,2] and it also worked for some ligands discussed here. However, as recently concluded, the effectiveness of the method depends strongly on the nature of the ligand.[3] We assume that the reason for this is the limited solubility of specific ligands in acetone/water mixtures (the medium used to precipitate the NPs) and EtOH (the solvent used for sample rinsing).

Surface-bound ligands can be distinguished from the corresponding free ligand molecules by the shift of NMR resonances of bound ligands due to the influence of NP metal core.[4,5] The Pt NPs functionalized with L-alanine (ALA, Fig. S1), L-(+)-2-aminobutyric acid (ABA, Fig. S3), L-valine (VAL, Fig. S5), L-*tert*-leucine (*tert*-LEU, Fig. S7), and L-phenylglycine (PHG, Fig. S8) gave two sets of ^{1}H signals. This means that not all non-bound ligands could be removed for these samples. However, the ratio of the NMR signal intensities (see Figures below) of free to surface-bound ligands does not represent the actual ratio of the two ligand species in the samples. In order to achieve the highest possible signal-to-noise ratio for surface-bound ligands, supersaturated NP dispersions were prepared for NMR analysis. As the solubility of the ligands is higher than the dispersibilities of the NPs, the ratio of free to surface-bound ligands that is detected by NMR is higher than their actual ratio in the original catalyst sample. In order to assign the signals to either Pt-bound ligands or free ligands, pure ligands were added to the dispersions leading to an increase of the signals that correspond to the free ligand molecules. In addition, all samples contain organic impurities (not numbered signals in the NMR spectra shown below) which may originate from the different organic solvents used during the sample preparation. Due to the low NMR signal intensities of the surface-bound ligands the signals of the organic impurities appear strongly pronounced like the free ligands.

The ^{1}H NMR spectrum of Pt NPs functionalized with L-threonine (THREO, Fig. S9a) shows, beside some organic impurities, only one set of signals that can be assigned to the ligand. This indicates successful removal of non-binding ligands by rinsing with EtOH for this sample. In order to discriminate whether this signal pattern is related to free or Pt-bound ligands, the corresponding pure amino acid was added (Fig. S9b). The appearance of a second set of signals demonstrates that THREO is indeed bound to the metal surface.

In order to further support our assignment of the observed signals, two-dimensional NMR experiments (*HH*-COSY) were carried out. Correlations in the *HH*-COSY spectrum allows for identification of signals that belong to the same molecule (see Fig. S2, S4, S6, S10).

Pt NPs functionalized with 4-fluoro-L-2-phenylglycine (F-PHG) could not be precipitated effectively. As a result, it was not possible to obtain the high quantities needed to record NMR spectra with sufficient signal-to-noise ratio.

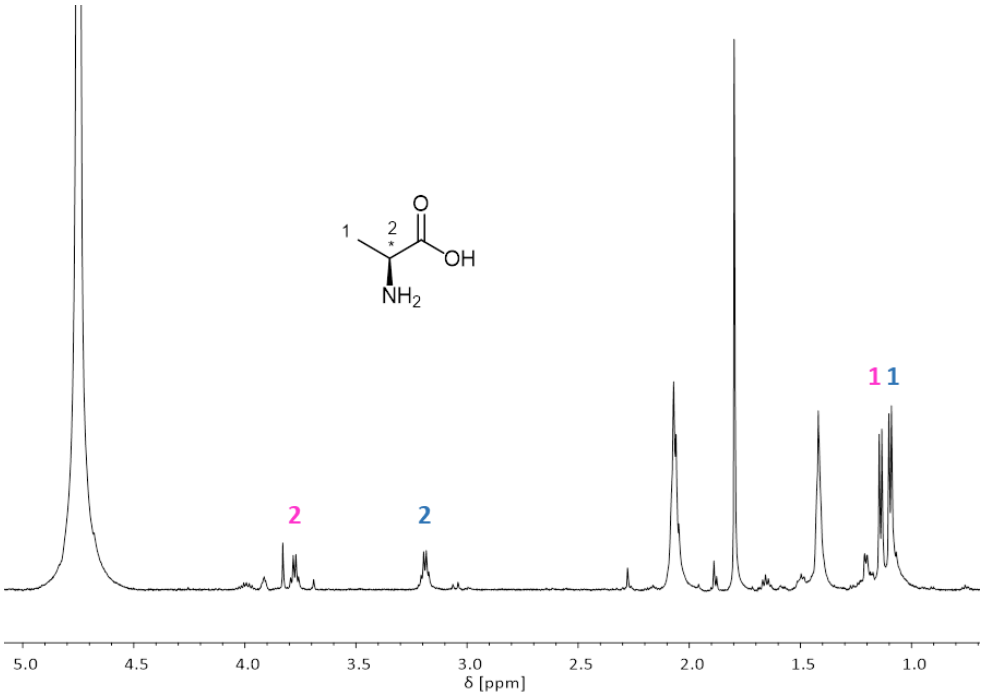

Figure S1. ^{1}H NMR spectrum (600 MHz, 300 K) in D_2O of a mixture of free ALA (see blue numbers) and Pt-bound ALA (see magenta numbers). Pure ALA shows two characteristic signals. The Pt-bound ALA shows the same signals, but being shifted. The shifts result from interaction with the metal core.

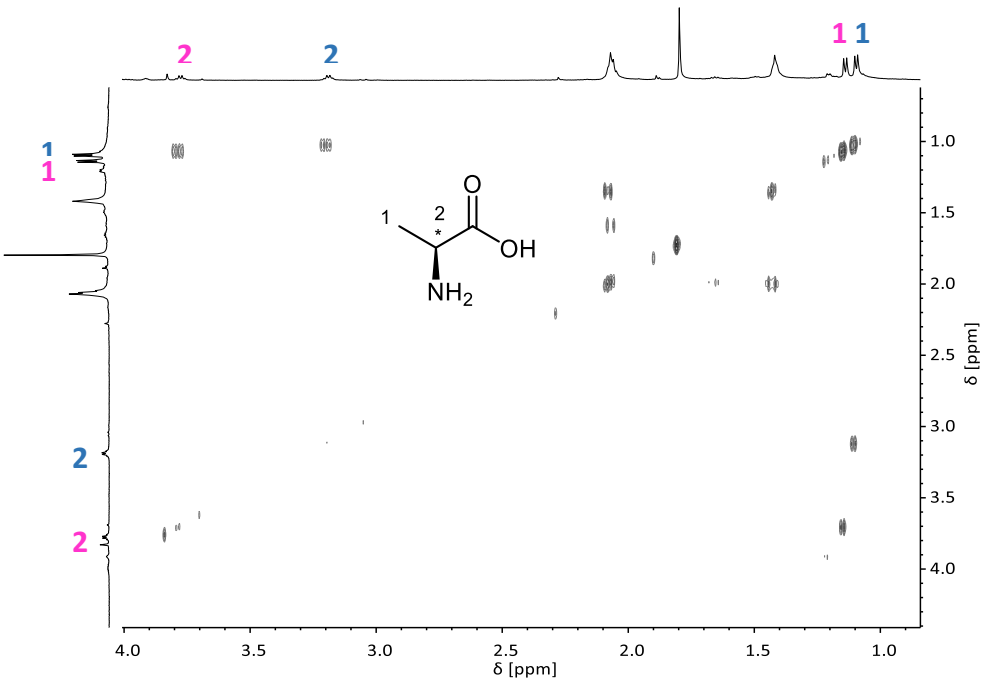

Figure S2. *HH*-COSY spectrum (600 MHz, 300 K) of a mixture of free ALA and Pt-bound ALA in D_2O. The identical correlations confirm that the Pt-bound ligand is indeed ALA.

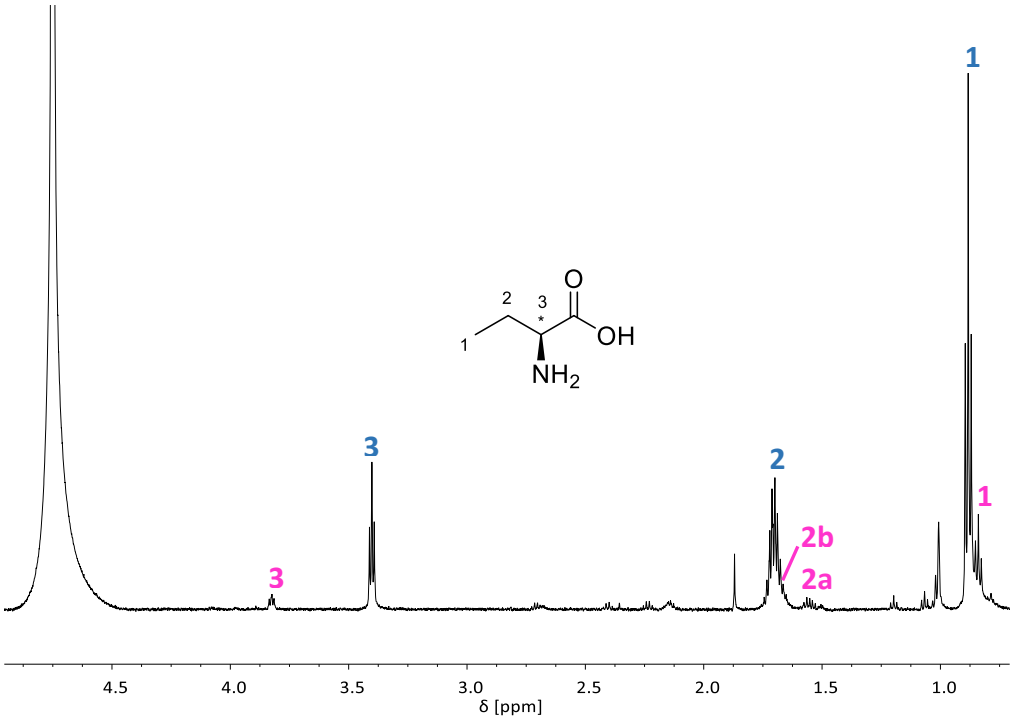

Figure S3. ^{1}H NMR spectrum (600 MHz, 300 K) in D_2O of a mixture of free ABA (see blue numbers) and Pt-bound ABA (see magenta numbers). Pure ABA shows three characteristic signals. Pt-bound ABA shows all the characteristic signals of ABA, but they are shifted; in particular, the proton being closest to the surface (3) shows a significant downfield shift due to the interaction with the metal core.

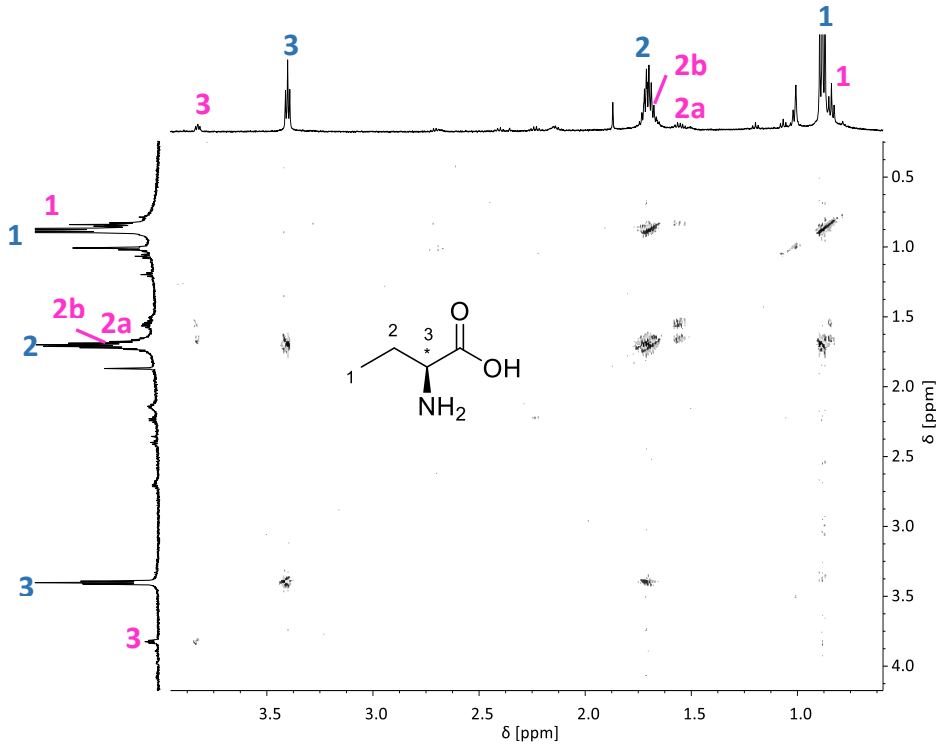

Figure S4. *HH*-COSY spectrum (600 MHz, 300 K) of a mixture of free ABA and Pt-bound ABA in D_2O. The identical correlations confirm that the Pt-bound ligand is indeed ABA.

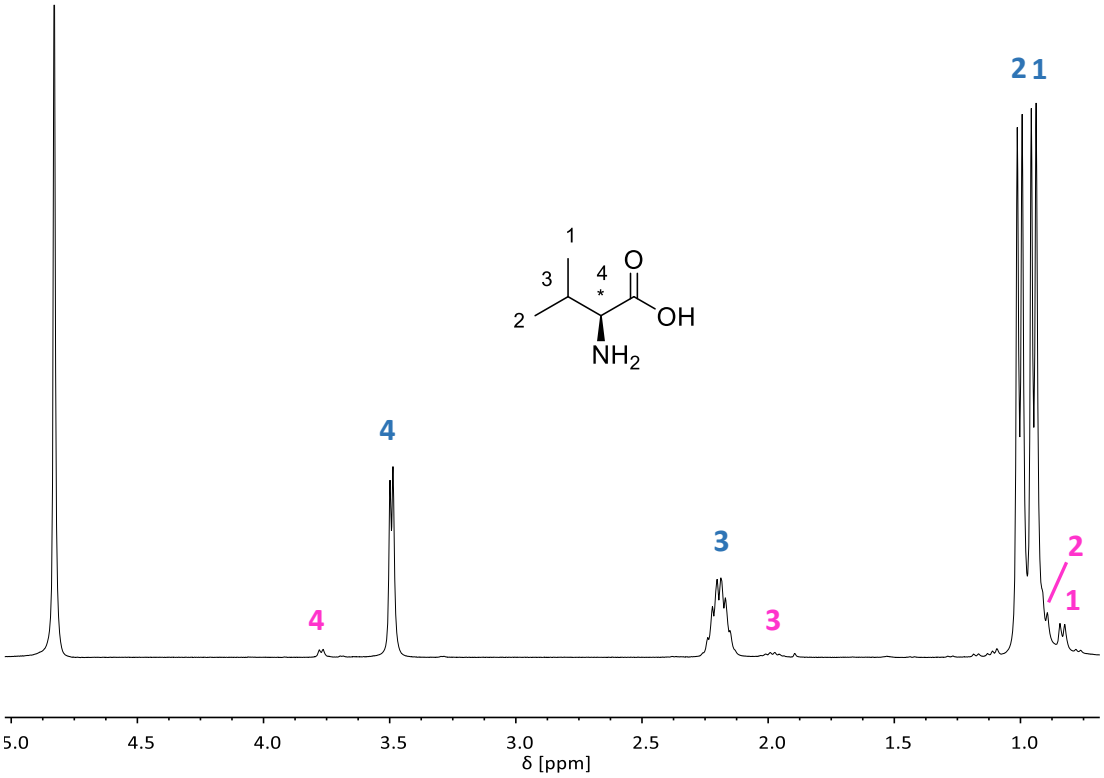

Figure S5. ^{1}H NMR spectrum (360 MHz, 293 K) in D_2O of a mixture of free VAL (see blue numbers) and Pt-bound VAL (see magenta numbers). Pure VAL shows four characteristic signals. Pt-bound VAL shows all the characteristic signals of VAL, but they are shifted; in particular, the proton being closest to the surface (4) shows a significant downfield shift due to the interaction with the metal core.

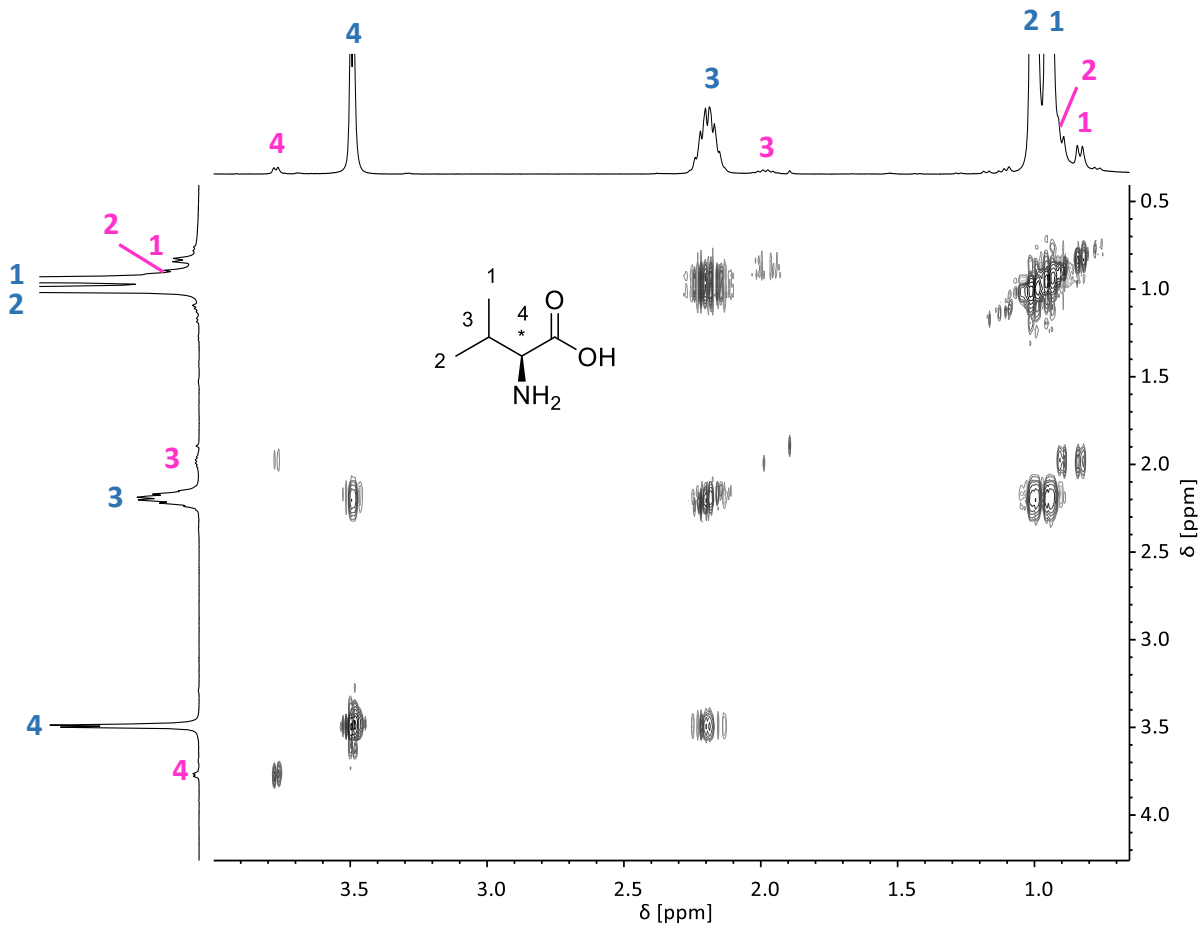

Figure S6. *HH*-COSY spectrum (360 MHz, 293 K) of a mixture of free VAL and Pt-bound VAL in D_2O. The identical correlations confirm that the Pt-bound ligand is indeed VAL.

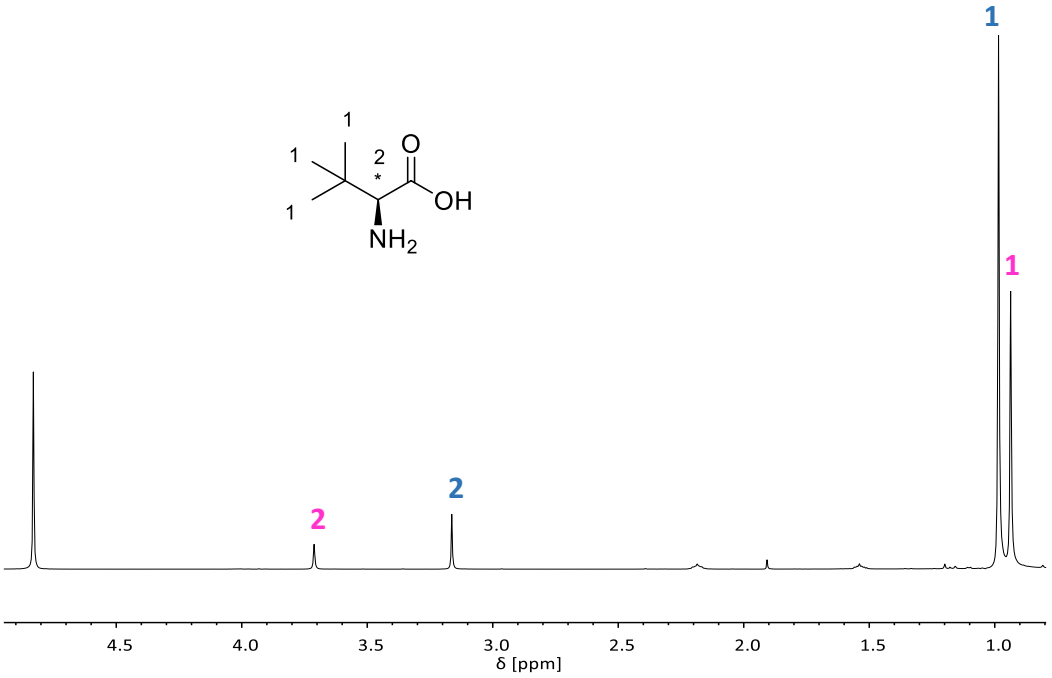

Figure S7. ^{1}H NMR spectrum (360 MHz, 293 K) in D_2O of a mixture of free *tert*-LEU (see blue numbers) and Pt-bound *tert*-LEU (see magenta numbers). The interaction of the Pt-bound ligands with the metal core leads to chemical shifts compared to the signals obtained for the free ligands. The proton being closest to the surface (2) shows a significant downfield shift.

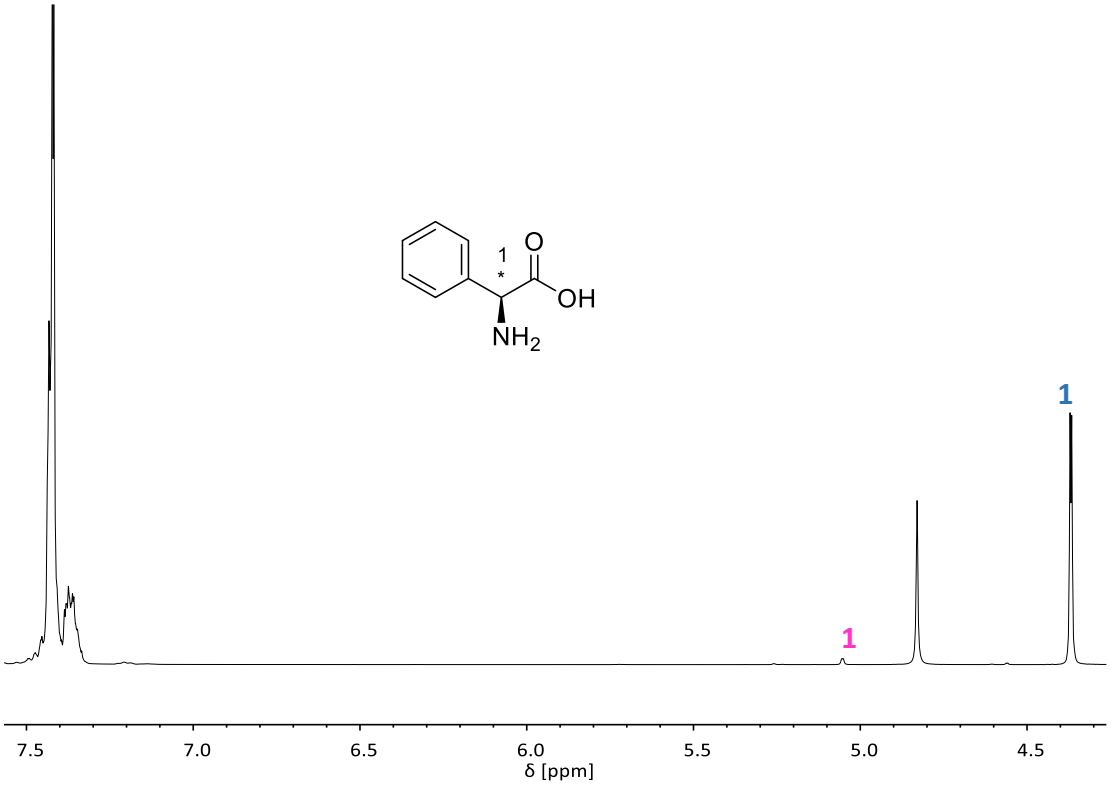

Figure S8. ^{1}H NMR spectrum (360 MHz, 293 K) in D_2O of a mixture of free PHG and Pt-bound PHG. The signals of the aromatic moiety are difficult to differentiate. However, the proton of Pt-bound PHG being closest to the surface (see magenta number 1) shows a significant downfield shift compared to unbound PHG (see blue number 1), which evidences that PHG is successfully bound to the Pt surface.

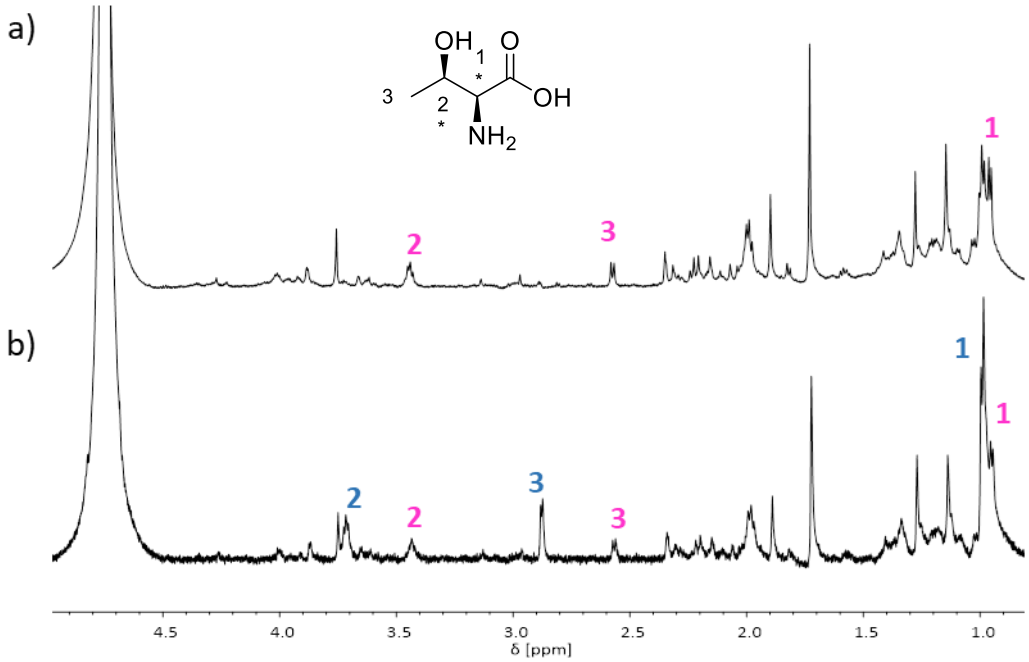

Figure S9. ^{1}H NMR spectrum (600 MHz, 300 K) in D_2O of Pt-bound THREO (a) and a mixture of free THREO (see blue numbers) and Pt-bound THREO (see magenta numbers) after addition of free ligand (b). The interaction of Pt-bound ligand with the metal core leads to different chemical shifts of the protons compared to the free ligand.

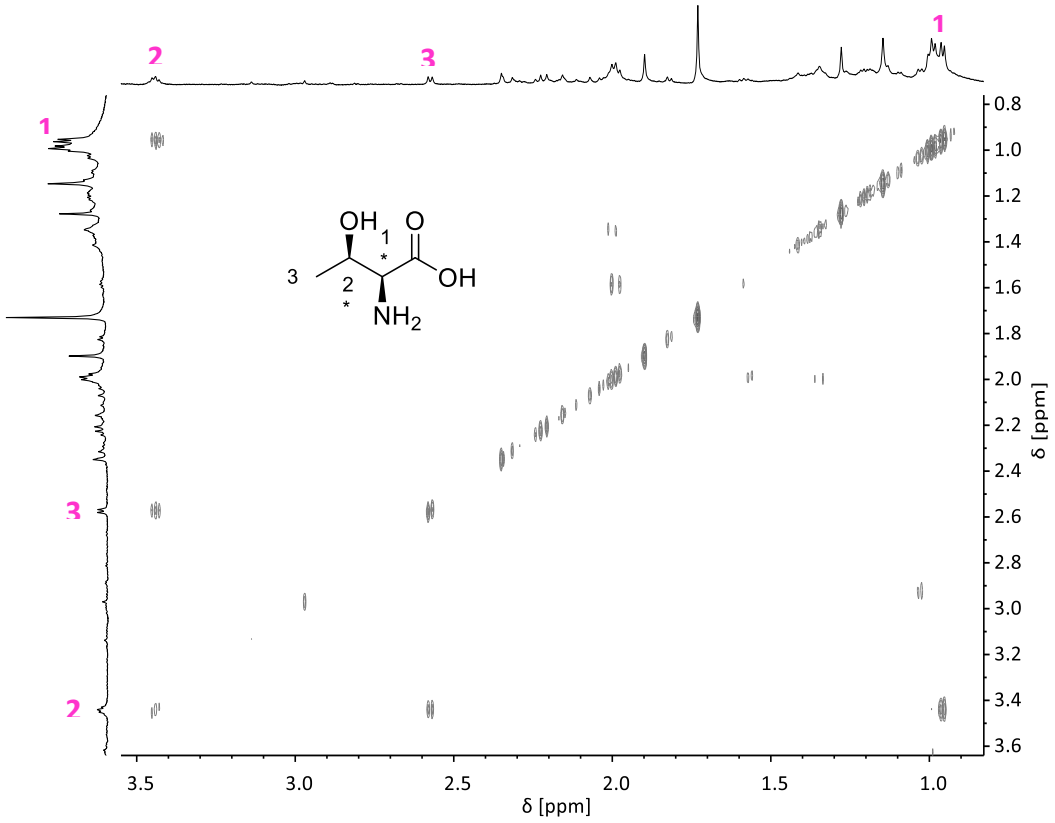

Figure S10. *HH*-COSY spectrum (600 MHz, 300 K) of Pt-bound THREO in D_2O. The identical correlations confirm that the Pt-bound ligand is indeed THREO.

2. Reaction Energy Profiles

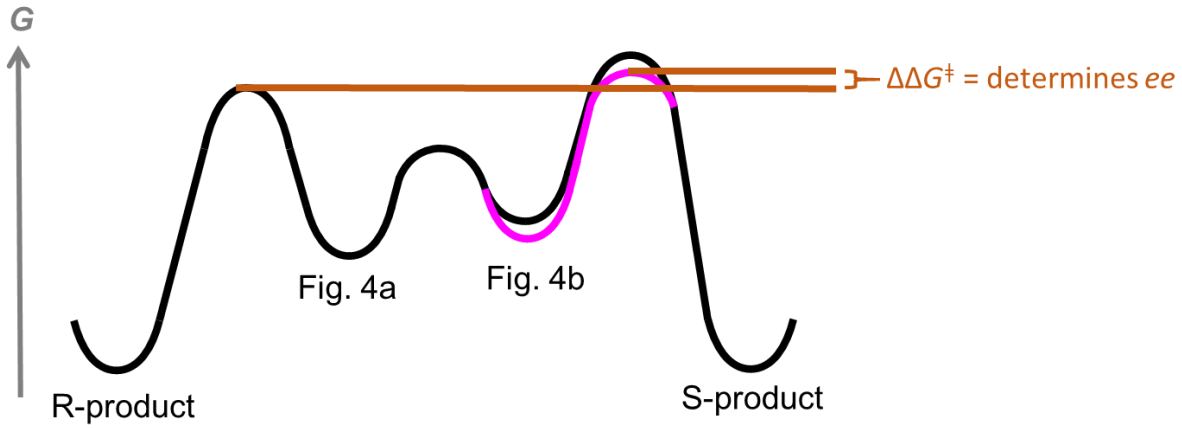

Figure S11. Illustration of the energy profile for the hydrogenation of ß-keto esters over THREO-functionalized Pt NPs. From the mode shown in Figure 3a R-product is formed (left), from the mode shown in Figure 4b the S-product is formed (right). A stabilization of the undesired binding mode (Fig. 4b) leads to shift of the energy potential curve to lower energies (see magenta curve in Fig. S11). $\Delta\Delta G^{\ddagger}$ and thus the *ee* decrease. The transition state in Figure 4a is still the lower laying one (see also the potential curve on the left of Fig. S11 compared to the magenta one on the right) so that the R-product is primarily formed one.

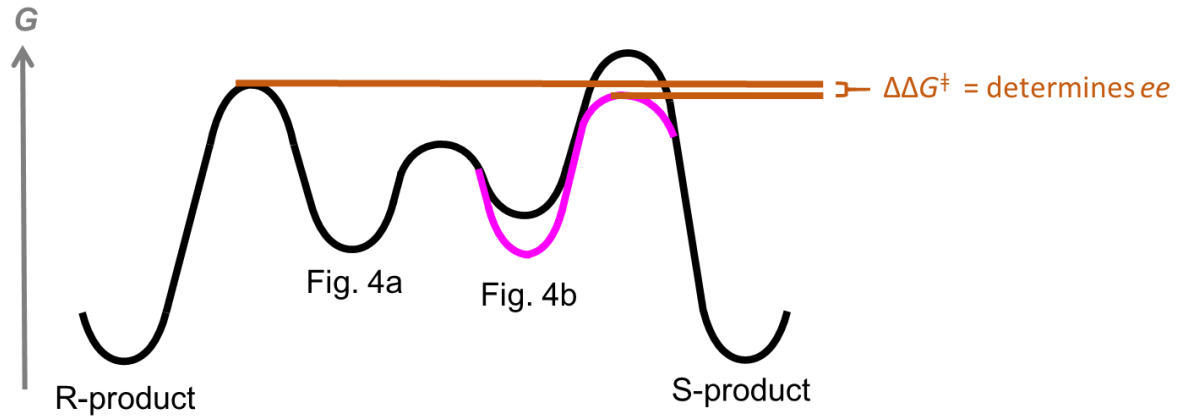

Figure S12. Illustration of energy profile that shows the effect of further stabilizing of the undesired binding mode. The transition state in Figure 4b is now the lower lying one and thus the product configuration changes. The S-product is primarily formed one.

3. Effect of Ligand and Reactant Structure on the Asymmetric Bias

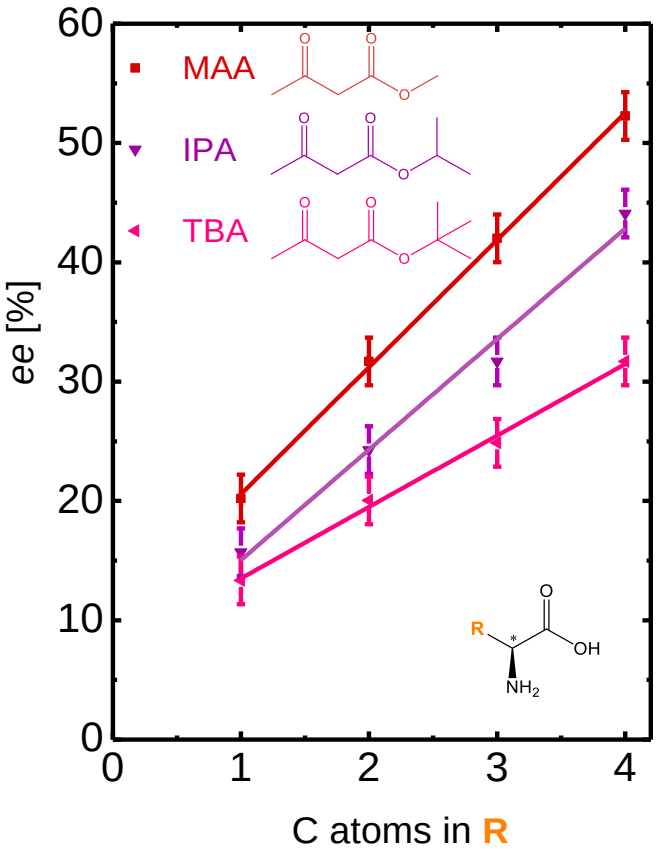

Figure S13. Influence of the size of the substituent R of the ligand on the stereoselectivity in the hydrogenation of ß-keto esters with OR'' groups of different steric demand – methylacetoacetate (MAA), isopropyl acetoacetate (IPA), and *tert*-butyl acetoacetate (TBA) (reactant structures are shown in the top left corner). By introducing bulkier R'' substituents the stereoselectivity decreases. However, for all three reactants the *ee* increases if the steric demand of ligand's R substituent is enhanced. The solid lines are linear fits of the experimental data and serve merely as guides to the eye.

From the *ee* values $\Delta\Delta G^{\ddagger}$ was calculated as follows:

$$ee = \frac{([R] - [S])}{([R] + [S])} * 100\% \quad (1)$$

$$[R] - ee[R] = [S] + ee[S] \quad (2)$$

$$[R](1 - ee) = [S](1 + ee) \quad (3)$$

$$\frac{[R]}{[S]} = \frac{(1 + ee)}{(1 - ee)} \quad (4)$$

According to the Curtin-Hammett principle the ratio of the two enantiomers can be written as[6]

$$\frac{[R]}{[S]} = e^{-\frac{\Delta\Delta G^{\ddagger}}{RT}} = \frac{(1 + ee)}{(1 - ee)} \quad (5)$$

$$-\frac{\Delta\Delta G^{\ddagger}}{RT} = \ln\left(\frac{1 + ee}{1 - ee}\right) \quad (6)$$

$$\Delta\Delta G^{\ddagger} = -RTln\left(\frac{1 + ee}{1 - ee}\right) \quad (7)$$

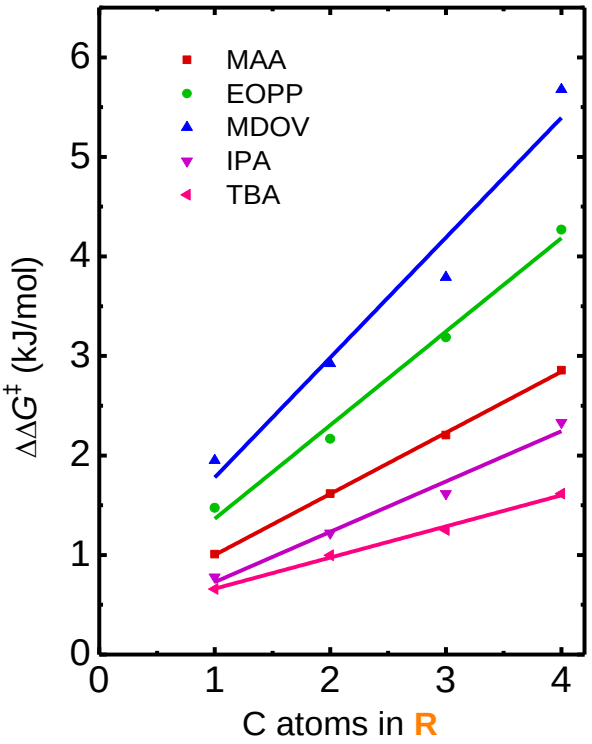

Figure S14. $\Delta\Delta G^{\ddagger}$ determined from the *ee* values. Changes in $\Delta\Delta G^{\ddagger}$ reveal that the interaction between R and R' is in the energy range of London dispersion interactions. The solid lines are linear fits of the calculated data and serve merely as guides to the eye.

Table S1. Comparison of stereoselectivities for the hydrogenation of EOPP and EFBA. An experimental error of ±2% has to be taken into account for the *ee*.

Ligand	*ee* [%] EOPP 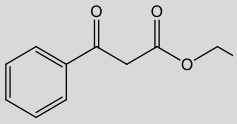	*ee* [%] EFBA 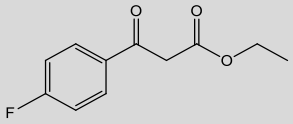
PHG 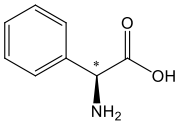	75	62
F-PHG 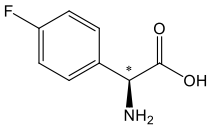	75	56

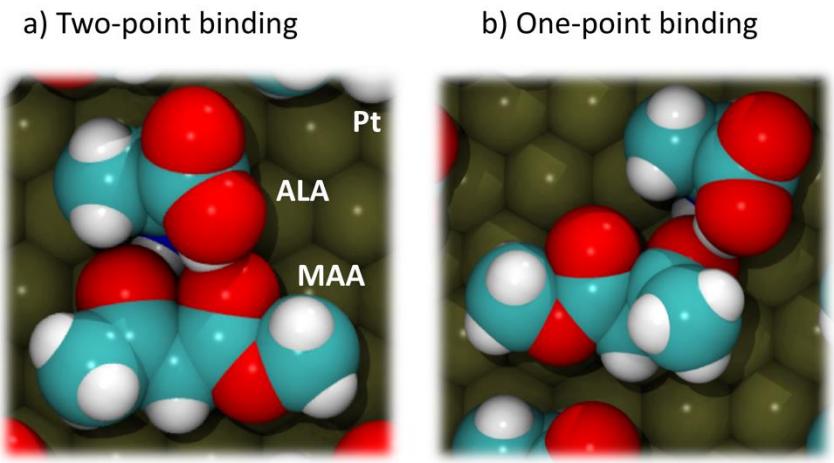

Figure S15. Two-point binding (see a) obtained by DFT simulation of the interaction of methylacetoacetate (MAA) with an alanine (ALA)–functionalized Pt(111) surface, without inclusion of the Grimme's dispersion correction. The diastereomeric counterpart (see b) was also modeled and consists of a one-point binding. vdW top view of the models. Color code: Pt, green; C, cyan; O, red; N, blue; H, white.

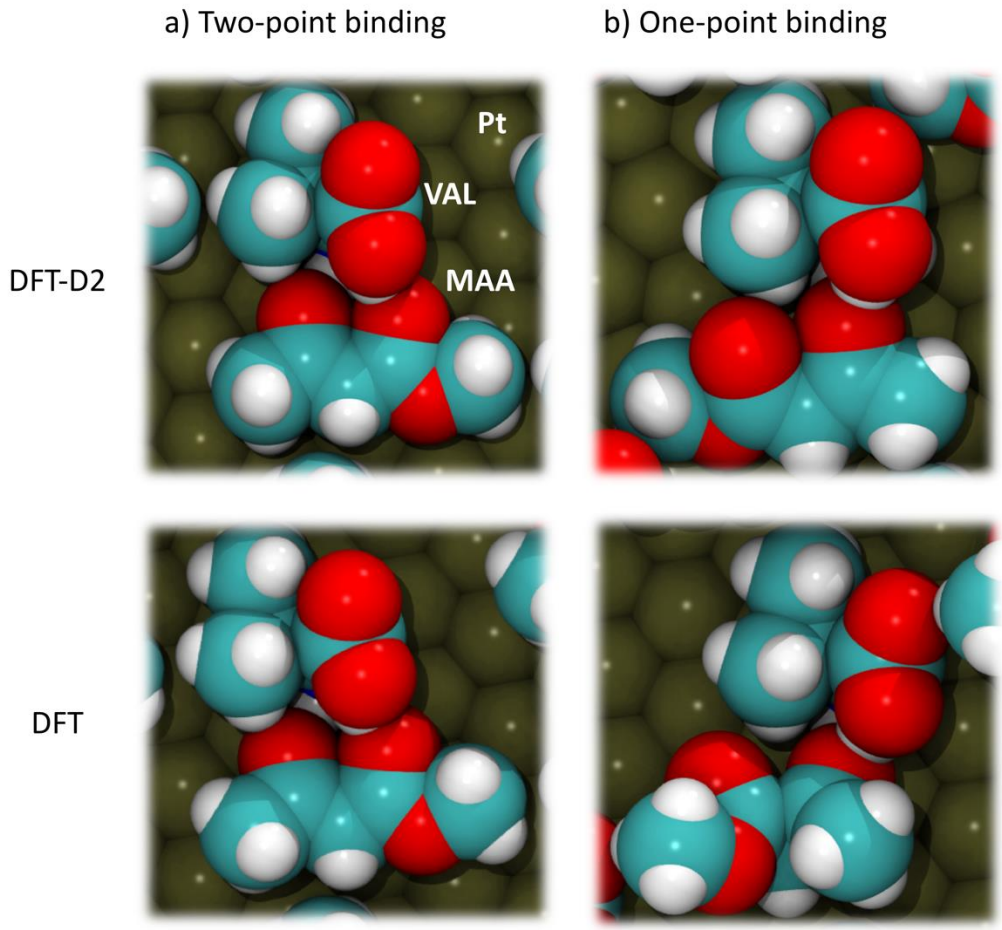

Figure S16. Two-point binding (see a) obtained by DFT simulation of the interaction of methylacetoacetate (MAA) with a valine (VAL)–functionalized Pt(111) surface, with (DFT-D2) and without (DFT) inclusion of the Grimme's dispersion correction. The diastereomeric counterpart (see b) was also modeled and consists of a one-point binding. vdW top view of the models. Color code: Pt, green; C, cyan; O, red; N, blue; H, white.

4. Extension of Reactant Scope

Table S2. Stereoselectivities for the hydrogenation of other reactants than ß-keto esters over ligand-functionalized Pt NPs. An experimental error of ±2% has to be taken into account.

reactant		*ee* [%] PRO	*ee* [%] *tert*-LEU	*ee* [%] PHG
methyl pyruvate (MP)	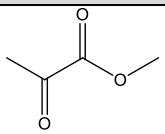	-5*	-2*	**
2,2,2-trifluoroacetophenone (TFA)	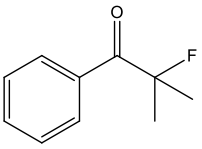	0	2	7
2-hydroxyacetophenone (HA)	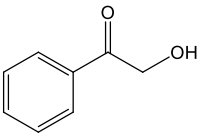	45	57	54
2-hydroxy-2-methylpropiophenone (HMP)	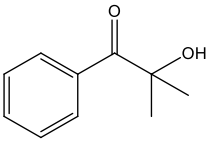	9	49	39

*(S)-enantiomer is primarily formed

**not examined

References

1 S. Kunz, M. M. Maturi, I. Schrader, J. Backenköhler, M. Tschurl and U. Heiz, *J. Colloid Interface Sci.*, 2014, **426**, 264–269.

2 I. Schrader, J. Warneke, J. Backenköhler and S. Kunz, *J. Am. Chem. Soc.*, 2015, **137**, 905–912.

3 I. Schrader, S. Neumann, A. Šulce, F. Schmidt, V. Azov and S. Kunz, *ACS Catal.*, 2017, **7**, 3979–3987.

4 Z. Wu, C. Gayathri, R. R. Gil and R. Jin, *J. Am. Chem. Soc.*, 2009, **131**, 6535–6542.

5 Tong, C. Rice, N. Godbout, A. Wieckowski and E. Oldfield, *J. Am. Chem. Soc.*, 1999, **121**, 2996–3003.

6 P. J. Walsh and M. C. Kozlowski, *Fundamentals of asymmetric catalysis*, Univ. Science Books, Sausalito, Calif., 2009.